Title

Identification and Characterization of Mitochondrial Subtypes in Caenorhabditis elegans via Analysis of Individual Mitochondria by Flow Cytometry

Journal

Analytical Chemistry, 88(12)

ISSN

0003-2700

Authors

Daniele, Joseph R
Heydari, Kartoosh
Arriaga, Edgar A
et al.

Publication Date

2016-06-21

DOI

10.1021/acs.analchem.6b00542

Peer reviewed

HHS Public Access

Author manuscript

Anal Chem. Author manuscript; available in PMC 2017 June 21.

Published in final edited form as:

Anal Chem. 2016 June 21; 88(12): 6309–6316. doi:10.1021/acs.analchem.6b00542.

Identification and Characterization of Mitochondrial Subtypes in *Caenorhabditis elegans* via Analysis of Individual Mitochondria by Flow Cytometry

Joseph R. Daniele[†], **Kartoosh Heydari**[‡], **Edgar A. Arriaga**[§,*], and **Andrew Dillin**[†]

[†]Department of Molecular and Cellular Biology, University of California, Berkeley, Berkeley, California 94720, United States

[‡]LKS Flow Cytometry Core, Cancer Research Laboratory, University of California, Berkeley, Berkeley, California 94720, United States

[§]Department of Chemistry, University of Minnesota, Minneapolis, Minnesota 55455, United States

Abstract

Mitochondrial bioenergetics has been implicated in a number of vital cellular and physiological phenomena, including aging, metabolism, and stress resistance. Heterogeneity of the mitochondrial membrane potential ($\Delta\psi$), which is central to organismal bioenergetics, has been successfully measured via flow cytometry in whole cells but rarely in isolated mitochondria from large animal models. Similar studies in small animal models, such as *Caenorhabditis elegans* (*C. elegans*), are critical to our understanding of human health and disease but lack analytical methodologies. Here we report on new methodological developments that make it possible to investigate the heterogeneity of $\Delta\psi$ in *C. elegans* during development and in tissue-specific studies. The flow cytometry methodology described here required an improved collagenase-3-based mitochondrial isolation procedure and labeling of mitochondria with the ratiometric fluorescent probe JC-9. To demonstrate feasibility of tissue-specific studies, we used *C. elegans* strains expressing blue-fluorescent muscle-specific proteins, which enabled identification of muscle mitochondria among mitochondria from other tissues. This methodology made it possible to observe, for the first time, critical changes in $\Delta\psi$ during *C. elegans* larval development and provided direct evidence of the elevated bioenergetic status of muscle mitochondria relative to their counterparts in the rest of the organism. Further application of these methodologies can help tease apart bioenergetics and other biological complexities in *C. elegans* and other small animal models used to investigate human disease and aging.

Graphical abstract

[*]**Corresponding Author**. arriaga@umn.edu.

ASSOCIATED CONTENT

Supporting Information

The Supporting Information is available free of charge on the ACS Publications website at DOI: 10.1021/acs.analchem.6b00542.

Supplemental experimental procedures, references, one table, and four figures (PDF)

The authors declare no competing financial interest.

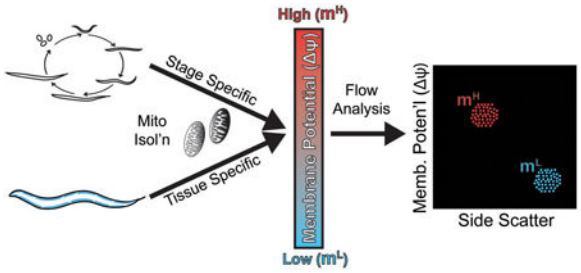

Understanding and measuring the bioenergetics of an organism is vital to the analysis and characterization of a wide array of cellular and physiological phenomena. Many of these processes, such as aging, metabolism, and stress-resistance, depend heavily on the functionality of mitochondria. Although it is clear that mitochondrial dysfunction is prevalent in brain, muscle, and liver[1,2] in multiple mitochondrial diseases, methodologies that are both widely applicable to diverse animal models and used to characterize mitochondrial heterogeneity and tissue-specific variation in mitochondrial function are lacking.

A central feature of mitochondrial function and bioenergetics is their membrane potential ($\Delta\psi$). Flow cytometry has been used to measure mitochondrial $\Delta\psi$ in single cells and in isolated mitochondria.[3–12] Although the identification and characterization of mitochondrial subtypes is paramount to understanding the pathology and tissue etiology of mitochondrial disease, the ability to isolate and characterize mitochondria and characterize mitochondrial $\Delta\psi$ from the nematode *Caenorhabditis elegans* (*C. elegans*), one of the most important biological models of disease and aging, has not been demonstrated.

In *C. elegans*, $\Delta\psi$ perturbation has been implicated in lifespan extension, fertility, apoptosis, and in a related species (*C. briggsae*) has been found essential to increased survival in tropical environments and resistance to stress.[13–18] Due to its small size, fast generation time, transparent cuticle, and multicellularity (nervous system, digestive system, musculature), *C. elegans* is an excellent biological model for various fields of biology, including aging and mitochondrial research. Most of the work linking mitochondrial characteristics to phenotypes in *C. elegans* has been done via microscopy. Studies utilizing isolated mitochondria are scarce, likely due to the lack of well-characterized and effective methods to isolate high quality mitochondria from nematodes, which possess a remarkably tough outer cuticle and distinct morphological features at each stage of development.

Although flow cytometry has been applied to analyzing isolated nematode mitochondria for reactive oxygen species,[19] here we define a new flow cytometry approach to (1) analyze the membrane potential of *C. elegans* mitochondria obtained through an improved isolation procedure and (2) demonstrate the potential of this approach to analyze isolated mitochondria from different larval stages and specific nematode tissue. With this approach, we characterize two mitochondrial subtypes, which arise during larval development and conclude that $\Delta\psi$ is higher in muscle than in mitochondria pooled from the entire organism. While we applied this approach to *C. elegans* because of its prevalence as a model for development, disease pathology, toxicity, and aging, it is envisioned that it could also be

applied to monitor the $\Delta\psi$ of mitochondria isolated from cell cultures, other model organisms, or tissue biopsies thereby providing a new tool to improve our understanding on the role of mitochondrial bioenergetics, which is critical in multiple fields of biomedical research.

EXPERIMENTAL SECTION

Worm Strains and Reagents

The worm strain used in most experiments was N2 wild-type obtained from the Caenorhabditis Genetics Center (Minneapolis, MN, U.S.A.). The ratiometric mitochondrial membrane potential sensor dye JC-9 (3,3′-dimethyl-a-naphthoxacarbocyanine iodide) (D-22421) and mitochondrial labeling dyes MitoTracker Red CMXRos (M-7512) and MitoTracker Green FM (M-7514) were purchased from Life Technologies (now Thermo Fisher), whereas valinomycin (V0627) and levamisole hydrochloride (31742) were from Sigma-Aldrich, and collagenase type 3 (collagenase 3, CLS 3- LS004182) was purchased from Worthington. Reagents used in worm lysis included Protease Inhibitor (539134, Calbiochem), glass pasteur pipettes (9 in., VWR), a metal dounce grinder (2 mL, Wheaton), and a glass homogenizer (2 mL with small clearance pestle (0.07 mm), Kimble Chase).

Mitochondrial Isolation and Flow Experiments

Worm staging was performed at 20 °C in line with previously published developmental timing and worm growth media.[20,21] Before lysis, worms of the specified stages were washed off plates and resuspended in filter-sterilized Collagenase 3 buffer [100 mM Tris-HCl, pH 7.4, 1 mM $CaCl_2$] with or without Collagenase 3 enzyme (1 mg/mL) and gently agitated for 1 h at 20 °C.[22] Following treatment, the active collagenase was diluted out with 3 washes of autoclaved M9 [42 mM Na_2HPO_4, 22 mM KH_2PO_4, 86 mM NaCl, and 1 mM $MgSO_4.7H_2O$].

Mitochondria were isolated via a differential centrifugation protocol modified from Gandre and van der Bliek 2007.[23] To allow for depolarization, the mitochondrial isolation buffer was modified to include K^+ but still preserve osmolarity; filter-sterilized mitochondria isolation buffer (MIB) [50 mM KCl, 110 mM mannitol, 70 mM sucrose, 0.1 mM EDTA (pH 8.0), 5 mM Tris-HCl (pH 7.4), protease inhibitor]. It has been reported previously that isolated mitochondria can polarize and respire normally in the absence of an ETC substrate (e.g., succinate) as long as a “permeant ion” such as K^+ is present in the buffer.[24–26] Furthermore, the presence of this ion facilitates valinomycin (a K^+ ionophore) mediated depolarization of mitochondria. Of note, we found JC-9 dye to be incompatible with CCCP (or FCCP) because treatment with this depolarizing agent appeared to dramatically affect the amount of JC-1 in solution, which ultimately could alter the red/green ratio of mitochondria.[27] Perhaps this is why valinomycin has often been used in conjunction with JC dyes.[27–29]

Briefly, M9 from previous washes was replaced with MIB and worms were homogenized using a glass homogenizer for 18 strokes. In Figure 1, a metal dounce grinder was used to homogenize worms (also 18 strokes). Lysates were then transferred to Eppendorf tubes (using a glass Pasteur pipet) and JC-9 dye [final 10 μM] (or MitoTracker Red [final 10 μM]

for Figure 1) was added. Tubes were then spun at 200*g* for 5 min at 4 °C on a tabletop centrifuge. Supernatant was removed and transferred to new tubes and subsequently spun at 800*g* for 10 min at 4 °C. The supernatant from these tubes was spun once more at 12 000*g* for 10 min at 4 °C. Finally, this supernatant was removed, and mitochondria pellets were resuspended in filtered MIB and kept on ice before running on the flow cytometer (or prepared for Western blotting). For flow experiments, a portion of the resuspended mitochondria was reserved and set aside on ice. Once all samples were run, valinomycin [final 10 uM] was added to these set-aside tubes 3–5 min before each tube was run. All "depolarized" sample controls were run in this manner. A tube containing filtered MIB and JC-9 (or MitoTracker Red) alone was also included in these spins to use as a dye-alone control to run during flow experiments. Another tube with lysate but no JC-9 was also included in the spins to control for unlabeled mitochondria.

Data Acquisition and Statistical Analysis

Flow data was acquired using an LSR Fortessa Analyzer using the forward scatter (FSC), side scatter (SSC, Granularity) (488 nm/10), Pacific Blue (Blue channel) (450 nm/50), FITC (Green channel) (525 nm/50 with a 500 nm Long Pass filter), and PE-Tx-Red YG ("Red channel") (610 nm/20 with a 600 nm Long Pass filter) filters. Although all data points were recorded, lasers and acquisition settings were calibrated to nullify any signal from unlabeled mitochondria in the fluorescent channels used. For all experiments, only singlets (or single mitochondria) were used when creating any plots or performing any statistical analyses. FlowJo v10 was used to process the data and prepare contour plots. A black background provided a better contrast for visualization of multiple contour lines. For the experiments using blue-labeled (BFP-positive) mitochondria, only blue fluorescent mitochondria that had blue signal and green signal (to indicate JC-9 labeling) above background were counted as BFP positive mitochondria. Microsoft Excel (with the Sigma XL add-on) was used to perform statistical analyses. Significance testing was performed using the *t* test for comparison between means and the nonparametric Mann–Whitney test was performed for comparisons between medians. Error bars were included in select figures to represent the standard error of the Mean (SEM) or the median absolute deviation (MAD) when means or medians, respectively, were the main output. Error bars were included when not significant (ns) comparisons prevailed (see Figures 1B, 3D, 3E, 3F, S1B, S1C, S1D, and S3E). For comparisons that proved statistically significant we included only symbols (e.g., * = $p < 0.05$) to indicate the level of significance. This decision was based on the observation that inclusion of error bars and significance symbols in most graphs made it difficult to understand the data visually. With respect to mitochondrial morphology measurements, mitochondrial diameter was determined by extrapolating from forward scatter (FSC) data acquired using standard beads from Duke Standards (NIST Traceable Polymer Microspheres, catalog nos. 3K-100, 3K-200, 3K-400, 3K-700, and 3K-1000). To determine the best predictor of size, best fit regressions of FSC or side scatter (SSC) size versus bead diameter indicated a better fit for FSC [mitochondria diameter (nm) = $126.41*(\text{FSC})^{0.2386}$; $R^2 = 0.998$, residual sum of squares (RSS) = 791.26; versus $R^2 = 0.996$, RSS = 37 600 for SSC]. This is consistent with the preferred use of FSC to approximate mitochondrial size.[26,30,31]

RESULTS AND DISCUSSION

Collagenase 3 Treatment Enhances Yield in *C. elegans* Mitochondrial Isolation

Conventional isolation protocols for *C. elegans* mitochondria, using glass or metal homogenizers and differential centrifugation,[13,19,32,33] result in partial release and purification. Losses due to adherence of mitochondria to debris (e.g., the cuticle), destruction during homogenization, and centrifugation steps, reduce the yield of isolated mitochondrial mass. In addition, cosedimentation of subcellular components during differential centrifugations results in contamination of mitochondrial preparations. We hypothesized that the tough cuticle on the nematode surface, which is hard to homogenize, reduces the effectiveness of the conventional isolation protocols. Thus, a procedure that "weakens" the cuticle prior to homogenization would likely improve the yield of release of mitochondria when using conventional homogenizers, which are the "gold standard" for isolation of *C. elegans* mitochondria. Here, we systematically compared three isolation protocols. This included homogenizing nematodes with (1) a metal dounce grinder, (2) a glass homogenizer with small clearance pestle (0.07 mm), and (3) treatment of worms with collagenase 3 for 1 h at 20 °C before lysing with the glass homogenizer used in (2). The third treatment was designed to partially digest the cuticle on the nematode surface with collagenase 3, thereby facilitating homogenization, and release of mitochondria. This isolation also used a glass homogenizer (e.g., refs 34,35), instead of the metal dounce grinder, because worms stick less to glass than other surfaces (e.g., metal). We performed these experiments on larval L1 worms and L4 worms (see Figure 1A) because they span the range for nematode size and allow for comparisons of mitochondria from somatic tissues. We did not use adult worms in these studies because L4 worms lack a germ line, whereas the adult nematode has eggs with high amounts of mitochondria that would bias the comparisons with other larval stages.

To estimate the purity and yield of mitochondria obtained under these three different isolation protocols, we performed Western blots on crude lysate (Lys) and mitochondrial (Mt) fractions (Figure S1A). For both L1 and L4 worms, the glass and collagenase protocol gave the least contamination from both cytoplasmic (α-tubulin) and nuclear (histone H3) markers, indicating that this disruption protocol is beneficial to reduce contamination. The average absolute yield determined by densitometric analysis of all the mitochondrial markers in the Western blot was (37 ± 8%, mean ± std dev (SD)). There were no statistical differences between developmental stages or homogenization methods, but a difference was observed between interactions of these two factors (Table S1). These results suggest the isolation protocol using collagenase treatment does not have a detrimental effect on the yield of mitochondrial mass and that it is equivalent to the other two established procedures. Surprisingly, this analysis suggests the isolation protocol using collagenase may have a distinct effect on the isolation of L1 and L4 mitochondria, which merits exploration at the individual mitochondrial level as described below.

Because Western analysis only indicates mitochondrial protein amount and not the number of "mitochondrial particles", we used flow cytometric counts of MitoTracker Red-positive mitochondria (e.g., number of mitochondria per minute) to estimate the relative efficacy of

the various homogenization methods (Figure 1B). Homogenization of L1 and L4 larval stages using a metal homogenizer led to the lowest number of mitochondria, which is expected because mechanical forces applied through contact with the metal surface are "harsh" on organelles. Lysing with a glass homogenizer on L1 worms yielded 1.3× increase in mitochondria number relative to metal homogenization, but this made little difference on L4 worms (~0.95× relative to metal homogenization). Treatment of worms for 1 h with collagenase 3 prior to lysis, however, increased mitochondria number 2.3× in L1 and 1.7× in L4 worms relative to metal homogenization. Furthermore, flow cytometric analysis indicated that mitochondria diameter (Figure S1C) and mitochondrial granularity (Figure S1D) were fairly consistent among the three homogenization methods (i.e., ≤ 11% variation between medians of each method). Although each method applied to each larval stage has a unique distribution (data not shown), the results suggest that the enzymatic treatment does not dramatically alter the properties of isolated mitochondria relative to isolations done without collagenase 3. Thus, we posit that collagenase 3 treatment prior to glass homogenizer lysis is a suitable isolation procedure that improves the yield of mitochondrial particles ~2× relative to other currently practiced protocols.

Lastly, we considered the effect of the collagenase treatment prior to disruption on mitochondrial respiration, a surrogate for mitochondrial function that is dependent on the mitochondrial membrane potential ($\Delta\psi$). Treatment with collagenase 3 for 1 h did not change O_2 consumption in whole worms, suggesting that this enzyme does not compromise mitochondrial respiration prior to the application of any disruption procedure (Figure S1B). It is important to note that all mitochondrial isolation procedures disrupt the mitochondrial network, observed in vivo (e.g., by confocal fluorescence microscopy), resulting in the release of discrete "mitochondrial particles" that are functionally distinct from the original mitochondrial network. Thus, functional measurements done on isolated mitochondrial particles (in vitro) are highly associated but cannot be quantitatively compared to their in vivo counterparts, even when both approaches are widely used in mitochondrial studies.[36,37] On the other hand, similar respiration between collagenase-treated and nontreated worms suggests that their mitochondrial networks are functionally similar and that mitochondria isolated from such worms using either disruption method would provide equivalent representation of $\Delta\psi$ measurements on isolated mitochondria.

Membrane Potential in Isolated Mitochondria

Mitochondrial membrane potential ($\Delta\psi$) has been measured via flow cytometry in isolated mitochondria using indicator dyes like JC-9.[8–12] JC-9 is a ratiometric mitochondrial membrane potential probe that accumulates in the mitochondrial matrix as both a green "monomeric" and a red "aggregate" fluorescent form. This small cyanine dye freely crosses cell membranes and is driven into interior-negative membrane-bounded organelles, which possess lipophilic structures (e.g., hydrophobic protein domains and membranes). JC-9, unlike a similar lipophilic cation dye JC-1, has a higher affinity for lipids which enables its monomer to accumulate in the matrix independent of membrane potential. Formation of the red aggregate state, conversely, increases as mitochondria become more polarized (Figure 2A).[38]

In this study, JC-9 red fluorescence was easily distinguishable from either fluorescent aggregates of JC-9 or fluorescent aggregates of valinomycin (a K^+ ionophore used to depolarize mitochondria) which both form in the absence of mitochondria (Figure 2B, blue and Figure S2A, red, respectively). These various aggregates and unlabeled mitochondria (Figure 2B, orange and Figure S2A, blue) were effectively gated out using the green and red channels (see Experimental Section) from JC-9 labeled, isolated mitochondria (Figure 2B, red and Figure S2A, orange).

To confirm the response of JC-9 labeling to depolarization, JC-9 labeled mitochondria were depolarized using the K^+ ionophore valinomycin and distinguished from their polarized counterparts (Figure 2C and S2B). As described in the previous paragraph, labeled mitochondria were easily selected by gating in both the green and red channels. The respective fluorescence signals of polarized mitochondria increased 23- and 152-fold relative to controls (e.g., JC-9 alone, JC-9 and valinomycin alone, and unlabeled mitochondria, whereas the respective fluorescence signals of depolarized mitochondria increased 13- and 11-fold relative to controls (Figure S2G). Furthermore, we observed that green fluorescence intensity was minimally influenced (~20%) upon exposure to valinomycin (Figure S2C and S2D), whereas the red fluorescence intensity (Figure S2C′ and S2D) decreased dramatically (~38%) under depolarizing conditions. Previously reported analyses of "total" mitochondrial $\Delta\psi$ in single cells labeled with JC-1 made similar observations and demonstrated that ratiometric comparison of red to green fluorescence signals were well-suited to describe differences in polarization status of mitochondria in whole single cells.[38] Similarly, in this study, we observed that the ratio of JC-9 fluorescence of red aggregates to green monomers (which factors in organelle size), is sensitive to the polarization status of mitochondria, which suggests that it is a suitable indicator to monitor the magnitude of $\Delta\psi$ in isolated mitochondria (Figure 2D).

Forward and Side Scattering of Isolated Mitochondria

Because mitochondrial membrane potential has been associated with morphological characteristics,[26,30] we anticipated that FSC and SSC, used to derive size and granularity values, respectively (Figure S2E and Figure S2F, respectively), would further refine the energetic description of mitochondria. In agreement with previous observations,[26,30,31,39,40] we found superior prediction of size using FSC compared to SSC (see Experimental Section). In contrast, SSC, which we associated with the concept of "granularity",[26,30] has also been associated with mitochondrial bioenergetic state (e.g., polarization of the inner membrane, organelle swelling, or the state of ATP synthase in the mitochondrial membrane).[26,30]

Using the same depolarization procedure as in Figure 2C, we observed an 1.2× increase in mitochondrial size (Figure S2E) and 2.9× increase in granularity (Figure S2F). Although depolarizing agents can cause dramatic changes (e.g., Ca^{2+} depolarization of mitochondria results in dramatic swelling and disappearance of inner membrane structure[41,42]), depolarization with valinomycin and K^+ was reversed in minutes by removal K^+ from the depolarizing buffer. This observation is consistent with previous studies reporting minimal increase in FSC but a significant increase in granularity following depolarization with

valinomycin[26,30] and electron microscopy observations reporting a small increase in swelling and a dramatic increase in heavy metal-staining ("density" of lipids and/or proteins that bind heavy metals, e.g., Fe^{2+} binding in Complex II) in the matrix.[41] Thus, FSC and SSC further define changes associated with the energetic status of these organelles.

Mitochondrial Subpopulations in Worm Development

Mitochondria must play different roles during the major stages of nematode development (Figure 1A), but the lack of technologies has limited the study of mitochondrial energetic status during larval stages. Other unrelated systems, such as immortalized hippocampal neuroblasts[43] and perinatal development of rat liver,[44] show prevalence of a transient mitochondrial subtype with high $\Delta\psi$. Thus, we hypothesized that similar mitochondrial subtypes are present during the differentiation/expansion of new tissues such as the nervous system[45,46] and germ line[47,48] in *C. elegans*. Indeed, when we characterized these mitochondria, we found that $\Delta\psi$ had significant changes between adjacent larval stages of development. Such changes were more dramatic in the early stages reaching a maximum $\Delta\psi$ around the larval L2 (~50-fold higher) and then decreasing to display relatively minor changes from L4 to Day 2 (Figure 3A, white bars, and S3B). Granularity also had significant changes between adjacent larval stages of development and its overall profile resembled closely that of $\Delta\psi$ (Figure 3B, white bars, and S3D). Although much less dramatic than the changes observed in $\Delta\psi$ and granularity, mitochondrial size also varied significantly between adjacent stages (Figure S3A and S3C). Together, these observations suggest that mitochondria at an early stage of development may be in a different metabolic state.

When mitochondria were depolarized, the distributions of mitochondrial $\Delta\psi$ were consistent across developmental stages (Figure S3E and S3F). On the other hand, size and granularity of mitochondria in the depolarized state were more variable than $\Delta\psi$ (Figure S3G and S3H, respectively). Thus, we used the low $\Delta\psi$ range of mitochondria (or m^L) defined by depolarized mitochondria (white line in Figure 3C and Figure S3F) to define a threshold of mitochondrial subtypes. Mitochondria with $\Delta\psi$ above this threshold were defined as high $\Delta\psi$ (or m^H) subtype. Thus, the depolarization threshold made it possible to define the fraction of each mitochondria subtype (Figure 3D), which in turn were analyzed for individual mitochondrial $\Delta\psi$ measurements of different larval stages (Figure 3E,F).

As Figure 3D suggests, the m^H subtype was present at all stages of development, but its relative abundance changed between adjacent stages. In egg mitochondria, the m^H subtype was ~13%, but then its relative abundance significantly increased in L1 (55%) and L2 (56%) (see Figures S3B and S3D, yellow arrowheads) and then tended to go down starting at L3 (Figure 3D). Furthermore, separate analysis of m^L and m^H subtypes to compare changes between adjacent development stages, revealed that for both subtypes, L1 and L2 stage nematodes have the highest $\Delta\psi$, with the largest change occurring between eggs and L1. Not surprisingly, the key difference between the m^H and the m^L was the magnitude of $\Delta\psi$ at each stage of development (Figure 3E and 3F). Similar trends were observed for granularity (Figure S3J), but trends for mitochondrial size were significant but less dramatic (Figure S3I). Together, these results suggest that a subtype of mitochondria (m^H) at early stages of

development (LI, L2) has the capacity of sustaining Δψ's higher than those at the egg stage, L3–L4, or early adulthood (Day 1, Day 2).

What is the purpose of m^H mitochondria during early developmental stages (egg to L2)? Why does the relative abundance of m^H begin to decrease in the L3 stage to become a small percentage of the m^L mitochondria in the L4 stage? Given that m^H mitochondria have the molecular machinery to sustain high Δψ in vitro and have high granularity (Figure 3E and S3J, respectively), they may represent an active metabolic state in vivo, such as that in the presence of actively working ATP synthase.[26] This metabolic state may be uniquely needed during the differentiation/expansion of "new tissues" and is consistent with previous work that describes a mitochondrial subtype that arises during development.[43,44] Thus, our classification of mitochondria into m^H and m^L subtypes, and the consistency of our findings with previously reported observations, supports that the approach described here is adequate to monitor mitochondrial bioenergetics during development.

Membrane Potential Measurement of Muscle-Specific Mitochondria

Methodologies to characterize mitochondrial heterogeneity and tissue-specific variation in mitochondrial function in small models such as *C. elegans* are lacking. In response to this need, we extended the methodology described above to characterize the Δψ of mitochondria in the muscle of *C. elegans*. To distinguish muscle mitochondria, a blue fluorescent protein (BFP) was targeted to the mitochondrial matrix under the muscle-specific promoter, *myo-3* (Figure 4A). High-sensitivity, high-magnification confocal micrographs were taken to ensure the tissue specificity (Figure S4A and S4B) and proper mitochondrial targeting of this construct (Figure S4C). Mitochondria were isolated as previously described and flow cytometric analysis identified muscle mitochondria by their heightened blue fluorescence over mitochondria labeled with JC-9 alone and other controls. These mitochondria, identified as MLS::BFP Mito (JC-9) in Figure 4B, are clearly distinguishable from other mitochondria, identified as Mito (JC-9) in Figure 4B.

Muscle mitochondria (from L4 worms) had higher Δψ (Figure 4C and S4F), were significantly larger (~1.1× diameter, Figure S4D and S4G), and had more granularity (~1.9× SSC) (Figure S4E and S4H) than mitochondria isolated from all tissues. The size of isolated "muscle" mitochondria was very similar to mitochondrial diameter measurements previously reported in worm muscle (quantified using confocal microscopy ~900 nm diameter,[49] and ~916 nm by our flow measurements). Overall, these observations provide direct evidence that body wall muscle must be bioenergetically "ready" to respond to unusually high ATP demand.

CONCLUDING REMARKS

This report describes the first method to (1) analyze the individual Δψ of mitochondria obtained through an improved isolation procedure, (2) compare their individual Δψ at different larval stages, and (3) describe individual Δψ in a tissue-specific fashion in *C. elegans*, a critically important model of aging and disease. The use of highly sensitive flow cytometry enabled the distinction of mitochondrial properties (Δψ, size, granularity) at the individual organelle level, which was the basis of identification, classification, and

characterization of mitochondrial subtypes in two different biological *C. Elegans* paradigms. Using bulk assays, the method performs equally to conventional homogenization and isolation procedures showing similar yield of mitochondrial mass. Although sampling bias caused by the energetic status of the mitochondrial network in vivo prior to homogenization cannot be ruled out, the ability to characterize individual mitochondria into energetic subtypes consistent with other reports on mitochondrial energetics during development and tissue-specific demands, provides strong evidence for the applicability of this method. In fact, the method could be widely applicable to mitochondria isolated from any stage in the nematode lifespan (e.g., developing or aged animals), any tissue (e.g., muscle, intestine, neurons), or a combination of both applications (e.g., mitochondria from aged tissues). While we focused on JC-9 as an indicator of $\Delta\psi$, our protocols could be modified to use with other reporter dyes (e.g., MitoSOX to measure reactive oxygen species).

Although biological processes such as aging, metabolism, and stress resistance depend heavily on the functionality of mitochondria, established methodologies to measure tissue-specific variation in mitochondrial function in *C. elegans* are still lacking. Here we demonstrate that the reported methodology is capable of characterizing specifically muscle mitochondrial bioenergetics in this animal model. Given the relevance of this model to mitochondrial disease pathology and neurodegeneration, our methodology should enable future research to derive complex bioenergetics from a single tissue. While the muscle was showcased in this report, this method could be applied to any tissue of interest. Having the complement of tissue specific lines in muscle, neurons, and intestine, for instance, could allow one to comprehensively create nematode models of mitochondrial disease and then derive the tissue-specific components of mitochondria in aging and metabolism. While *C. elegans* was our main focus, we believe this method could also be applied to monitor the $\Delta\psi$ of mitochondria isolated from cell cultures, other model organisms, or tissue biopsies frequently used in a wide range of biological disciplines.

Supplementary Material

Refer to Web version on PubMed Central for supplementary material.

REFERENCES

1. Sharpley MS, Marciniak C, Eckel-Mahan K, McManus M, Crimi M, Waymire K, Lin CS, Masubuchi S, Friend N, Koike M, Chalkia D, MacGregor G, Sassone-Corsi P, Wallace DC. Cell. 2012; 151(2):333–343. [PubMed: 23063123]
2. Ylikallio E, Suomalainen A. Ann. Med. 2012; 44(1):41–59. [PubMed: 21806499]
3. Parone PA, Da Cruz S, Tondera D, Mattenberger Y, James DI, Maechler P, Barja F, Martinou J-C. PLoS One. 2008; 3(9):e3257. [PubMed: 18806874]
4. Cossarizza, A., Salvioli, S. Current Protocols in Cytometry. Hoboken, NJ: John Wiley & Sons, Inc.; 2001.
5. Gravance C, Garner D, Baumber J, Ball B. Theriogenology. 2000; 53(9):1691–1703. [PubMed: 10968415]
6. Chen H, Chomyn A, Chan DC. J. Biol. Chem. 2005; 280(28):26185–26192. [PubMed: 15899901]
7. Adhihetty PJ, Ljubicic V, Menzies KJ, Hood DA. Am. J. Physiol. - Cell Physiol. 2005; 289(4):C994–C1001. [PubMed: 15901602]

8. Smiley ST, Reers M, Mottola-Hartshorn C, Lin M, Chen A, Smith TW, Steele GD, Chen LB. Proc. Natl. Acad. Sci. U. S. A. 1991; 88(9):3671–3675. [PubMed: 2023917]
9. Saunders JE, Beeson CC, Schnellmann RG. J. Bioenerg. Biomembr. 2013; 45(1–2):87–99. [PubMed: 23080405]
10. Cossarizza A, Ceccarelli D, Masini A. Exp. Cell Res. 1996; 222(1):84–94. [PubMed: 8549677]
11. Vander Heiden MG, Chandel NS, Williamson EK, Schumacker PT, Thompson CB. Cell. 1997; 91(5):627–637. [PubMed: 9393856]
12. Narendra D, Tanaka A, Suen D-F, Youle RJ. J. Cell Biol. 2008; 183(5):795–803. [PubMed: 19029340]
13. Brys K, Castelein N, Matthijssens F, Vanfleteren JR, Braeckman BP. BMC Biol. 2010; 8(1):91. [PubMed: 20584279]
14. Kuang J, Ebert PR. Mitochondrion. 2012; 12(2):280–287. [PubMed: 22122855]
15. Lemire BD, Behrendt M, DeCorby A, Gášková D. Mech. Ageing Dev. 2009; 130(7):461–465. [PubMed: 19442682]
16. Tsang WY, Lemire BD. Biochem. Cell Biol. 2002; 80(5):645–654. [PubMed: 12440704]
17. Jagasia R, Grote P, Westermann B, Conradt B. Nature. 2005; 433(7027):754–760. [PubMed: 15716954]
18. Hicks KA, Howe DK, Leung A, Denver DR, Estes S. PLoS One. 2012; 7(8):e43837. [PubMed: 22952781]
19. Yang W, Hekimi S. PLoS Biol. 2010; 8(12):e1000556. [PubMed: 21151885]
20. Brenner S. Genetics. 1974; 77(1):71–94. [PubMed: 4366476]
21. Byerly L, Cassada RC, Russell RL. Dev. Biol. 1976; 51(1):23–33. [PubMed: 988845]
22. Cox GN, Kusch M, Edgar RS. J. Cell Biol. 1981; 90(1):7–17. [PubMed: 7251677]
23. Gandre S, van der Bliek AM. Methods Mol. Biol. 2007; 372:485–501. [PubMed: 18314747]
24. Gómez-Puyou A, Sandoval F, Chávez E, Tuena M. J. Biol. Chem. 1970; 245(20):5239–5247. [PubMed: 4319236]
25. Ogata E, Rasmussen H. Biochemistry. 1966; 5(1):57–66. [PubMed: 5940319]
26. Knight VA, Wiggins PM, Harvey JD, O'Brien JA. Biochim. Biophys. Acta, Bioenerg. 1981; 637(1):146–151.
27. Wolken GG, Arriaga EA. Anal. Chem. 2014; 86(9):4217–4226. [PubMed: 24673334]
28. Reers M, Smith TW, Chen LB. Biochemistry. 1991; 30(18):4480–4486. [PubMed: 2021638]
29. Cossarizza A, Baccaranicontri M, Kalashnikova G, Franceschi C. Biochem. Biophys. Res. Commun. 1993; 197(1):40–45. [PubMed: 8250945]
30. Beavis AD, Brannan RD, Garlid KD. J. Biol. Chem. 1985; 260(25):13424–13433. [PubMed: 4055741]
31. Petit PX. Plant Physiol. 1992; 98(1):279–286. [PubMed: 16668625]
32. Grad, L., Sayles, L., Lemire, B. Mitochondria. In: Leister, D., Herrmann, J., editors. Methods in Molecular Biology. New York: Humana Press; 2007. p. 51-66.
33. Kayser E-B, Sedensky MM, Morgan PG, Hoppel CL. J. Biol. Chem. 2004; 279(52):54479–54486. [PubMed: 15269213]
34. Frezza C, Cipolat S, Scorrano L. Nat. Protoc. 2007; 2(2):287–295. [PubMed: 17406588]
35. Fernández-Vizarra E, López-Pérez MJ, Enriquez JA. Methods. 2002; 26(4):292–297. [PubMed: 12054919]
36. Degli Esposti, M. Mitochondria. Pon, LA., Schon, EA., editors. Vol. 65. San Diego, CA: Academic Press; 2001. p. 75-96.
37. Cottet-Rousselle C, Ronot X, Leverve X, Mayol J-F. Cytometry, Part A. 2011; 79A(6):405–425.
38. Perelman A, Wachtel C, Cohen M, Haupt S, Shapiro H, Tzur A. Cell Death Dis. 2012; 3(11):e430. [PubMed: 23171850]
39. Lecoeur H, Langonné A, Baux L, Rebouillat D, Rustin P, Prévost M-C, Brenner C, Edelman L, Jacotot E. Exp. Cell Res. 2004; 294(1):106–117. [PubMed: 14980506]
40. Macouillard-Poulletier de Gannes F, Belaud-Rotureau M-A, Voisin P, Leducq N, Belloc F, Canioni P, Diolez P. Cytometry. 1998; 33(3):333–339. [PubMed: 9822344]

41. Yamada A, Yamamoto T, Yamazaki N, Yamashita K, Kataoka M, Nagata T, Terada H, Shinohara Y. Mol. Cell. Proteomics. 2009; 8(6):1265–1277. [PubMed: 19218587]
42. Shinohara Y, Almofti MR, Yamamoto T, Ishida T, Kita F, Kanzaki H, Ohnishi M, Yamashita K, Shimizu S, Terada H. Eur. J. Biochem. 2002; 269(21):5224–5230. [PubMed: 12392554]
43. Voccoli V, Colombaioni L. Brain Res. 2009; 1252:15–29. [PubMed: 19071097]
44. Medina JM, López-Mediavilla C, Orfao A. FEBS Lett. 2002; 510(3):127–132. [PubMed: 11801239]
45. Sulston JE, Horvitz HR. Dev. Biol. 1977; 56(1):110–156. [PubMed: 838129]
46. Sulston JE, Schierenberg E, White JG, Thomson JN. Dev. Biol. 1983; 100(1):64–119. [PubMed: 6684600]
47. Hirsh D, Oppenheim D, Klass M. Dev. Biol. 1976; 49(1):200–219. [PubMed: 943344]
48. Kimble JE, White JG. Dev. Biol. 1981; 81(2):208–219. [PubMed: 7202837]
49. Head BP, Zulaika M, Ryazantsev S, van der Bliek AM. Mol. Biol. Cell. 2011; 22(6):831–841. [PubMed: 21248201]

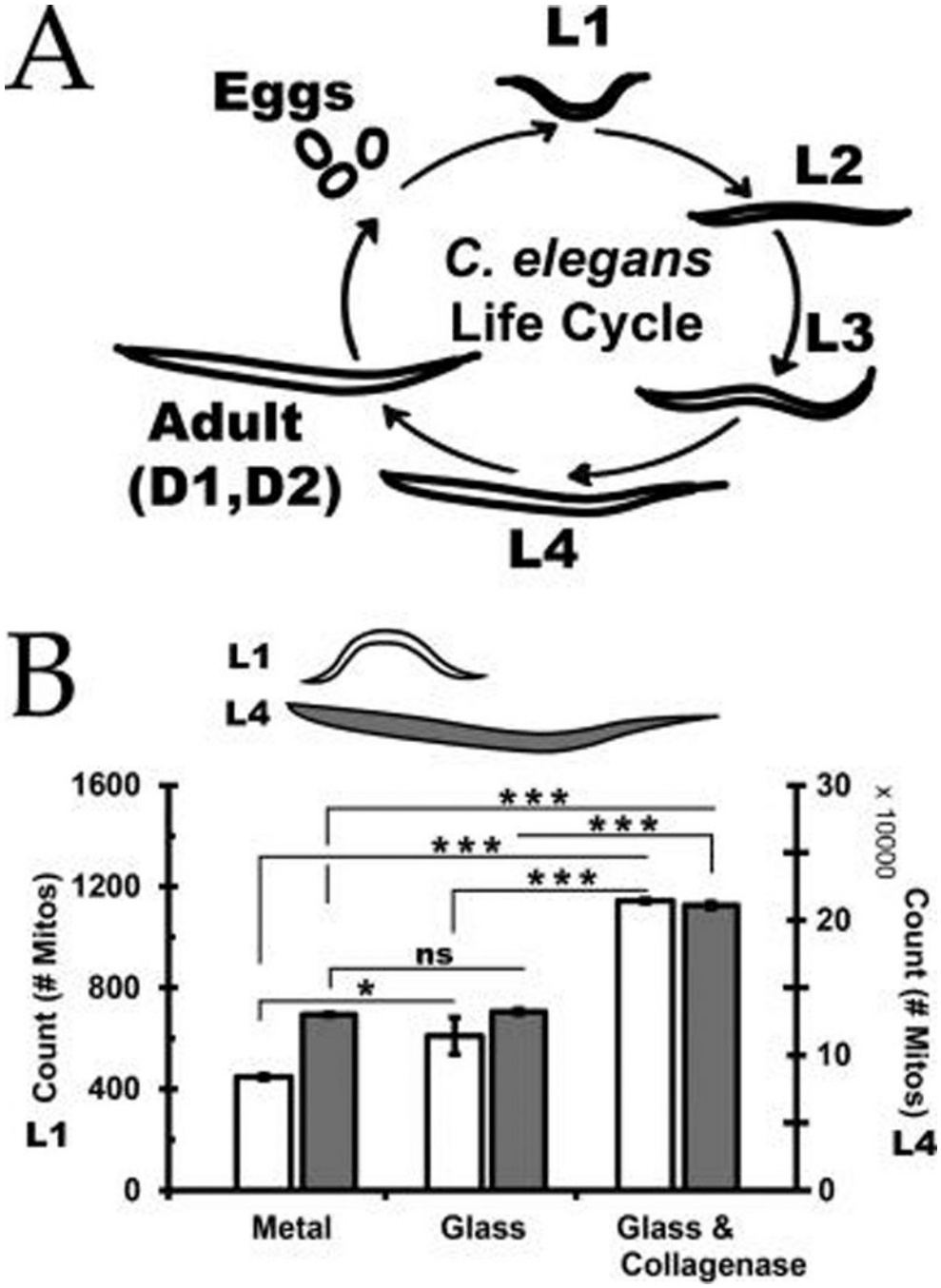

Figure 1.

Collagenase treatment enhances yield in *C. elegans* (worm) mitochondrial isolation. (A) Schematic of *C. elegans* life cycle to illustrate size and morphology differences. (B) Mitochondria were isolated from the L1 and L4 larval stages of worm development using either a metal dounce grinder (Metal), a glass dounce homogenizer (Glass), or a glass homogenizer following 1 h of collagenase 3 treatment (1 mg/mL) at 20 °C (Glass and Collag.). Bar plots depicting flow cytometric counts of MitoTracker Red (10 μM) positive mitochondrial yield (number of mitochondria per minute) from three technical replicates of

mitochondrial isolations from larval L1 (white bars) and L4 (gray bars) worms using the isolation techniques described above. Error bars are SEM from three technical replicates. * = $p < 0.05$, *** = $p < 0.0001$, and ns = not significant.

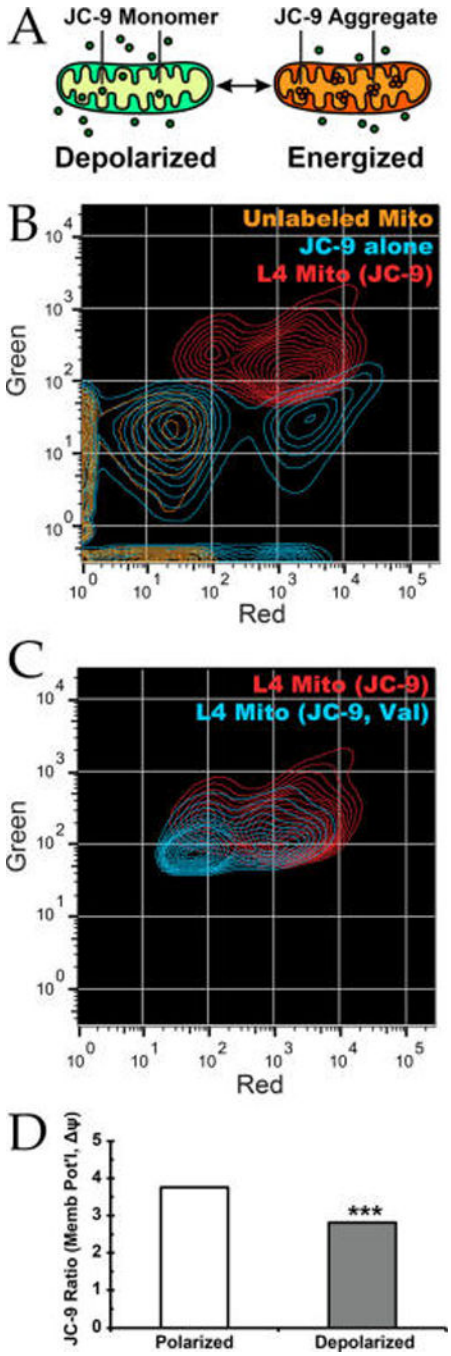

Figure 2.

JC-9 can label both polarized and depolarized isolated mitochondria. (A) JC-9 is a mitochondrial (Mito) dye that exists in a monomeric (green fluorescent) state but forms red fluorescent aggregates when mitochondria are polarized. Red fluorescence intensity increases as the mitochondrial membrane potential (Δψ) increases. (B) Contour plot showing separation of mitochondria from specific JC-9 dye aggregates alone (Blue) and L4 stage isolated mitochondria labeled with (Red) or without (Orange) 10 μM JC-9. (C) Contour plot showing distribution of isolated mitochondria from L4 stage worms labeled

with JC-9 (Red) or with both JC-9 and the depolarizing ionophore valinomycin (10 μM) (Blue). (D) Representative use of the Red/Green JC-9 fluorescence ratio in a comparison of polarized and depolarized mitochondria. Median Red/Green JC-9 fluorescence ratio is ~1.3× higher for polarized mitochondria due to formation of more aggregate (red). $N = 26274$ mitochondria for polarized and $N = 5455$ mitochondria for depolarized. *** = $p < 0.0001$.

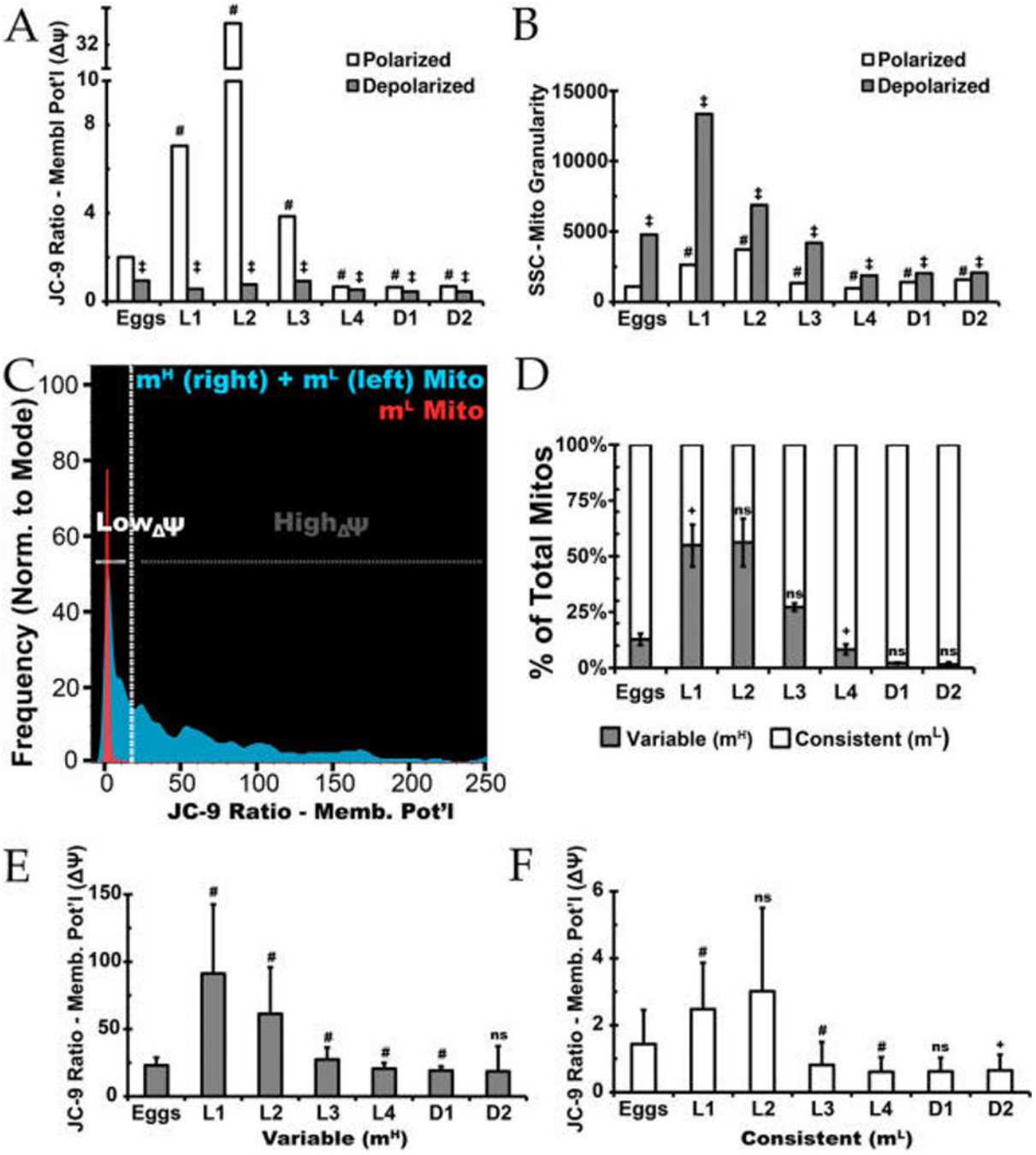

Figure 3.

Characterization of mitochondrial subpopulations in worm development. (A) Mitochondrial Δψ is relatively high during larval L1–L3 in *C. elegans* development and then falls. D1 and D2 stand for adult Day 1 and Day 2, respectively. Depolarization (gray bars) by valinomycin (12 μM) treatment reduces Δψ. (B) Mitochondrial granularity (side scatter, SSC) is relatively high during L1 to L3. For parts (A) and (B), # = $p < 0.0001$ relative to previous stage (e.g., L2 vs L1), ‡ = $p < 0.0001$ relative to polarized, mitochondria within a stage. (C) Using the L4-D2 JC-9 distribution profiles, and Δψ range under depolarizing conditions (see

Figure S3F), one can set a division point (white dotted line) to distinguish between m^H (variable) and m^L (consistent) mitochondrial subtypes. (D) Frequencies (% of JC-9 positive mitochondria) of high $\Delta\psi$ mitochondria (m^H) and low $\Delta\psi$ mitochondria (m^L) at each developmental stage. Values are averages from at least 3 biological replicates. Error bars are SEM, + = $p < 0.01$ relative to previous stage e.g. L2 to L1, and ns = not significant relative to previous stage. (E,F) Membrane potential, $\Delta\psi$, of both the m^H (3E, gray bars) and m^L (3F, white bars) throughout worm development. Values in bar charts are medians unless otherwise specified. # = $p < 0.0001$ relative to previous stage (e.g., L2 vs L1), + = $p < 0.01$ relative to previous stage e.g. L2 to L1, and ns = not significant relative to previous stage. Bars are median absolute deviation (MAD). For polarized mitochondria, $N = 34280$ for Eggs, 7963 for L1, 18586 for L2, 22313 for L3, 23497 for L4, 23476 for D1, and 45393 for D2. For depolarized mitochondria, $N = 11613$, 8137, 9965, 16035, 27394, 30069, and 29851 for Eggs – D2, respectively.

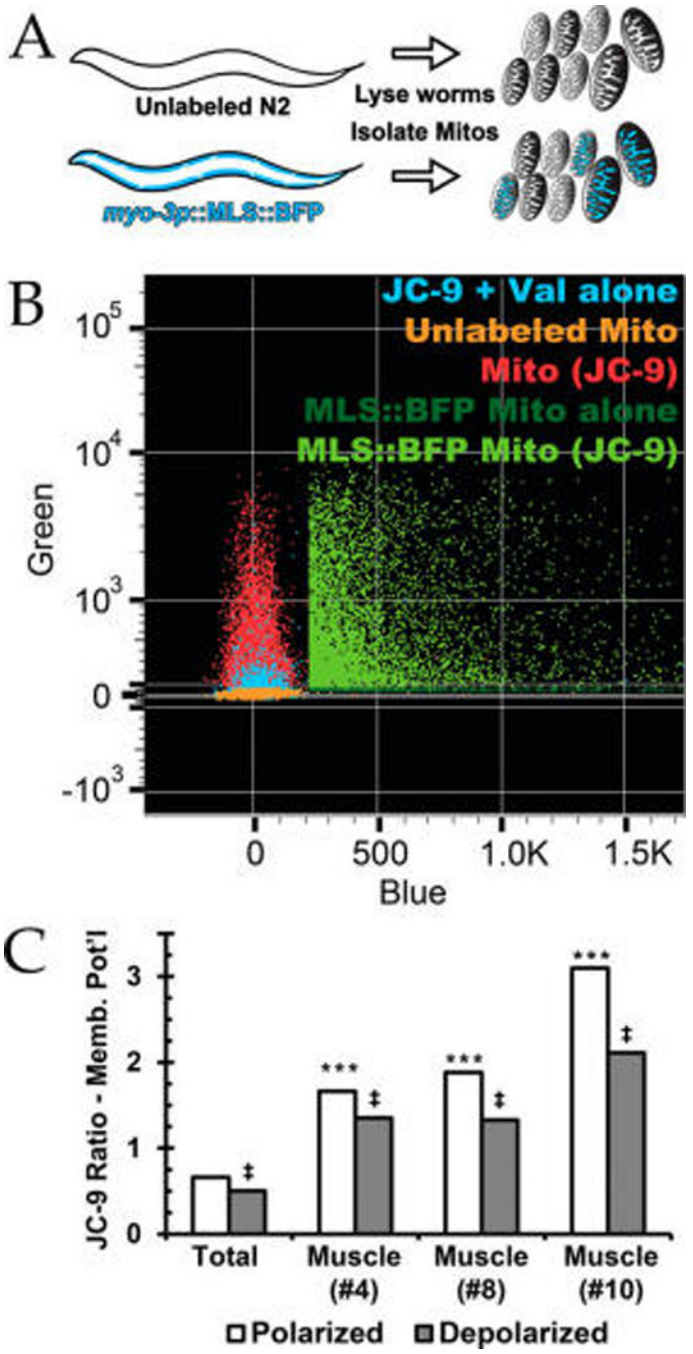

Figure 4.

Analysis of mitochondrial properties from specific *C. elegans* tissues. (A) At the L4 stage, unlabeled worms (empty worm) and worms expressing a blue fluorescent protein in their muscle mitochondria (blue worm) were lysed and mitochondria were isolated. (B) Flow cytometric analysis enabled the cutoff point (in the blue fluorescence channel) where only blue fluorescent mitochondria (which are also labeled with JC-9, light yellow) were detected. Relevant controls of JC-9 and valinomycin alone (blue), unlabeled mitochondria (orange), nonblue fluorescent mitochondria labeled with JC-9 (red), blue fluorescent

mitochondria alone (dark green) are included in the plot to demonstrate the heightened blue and green fluorescent signal of JC-9-positive muscle mitochondria (light yellow). (C) Measurement of polarized (white bars) and depolarized (gray bars) mitochondrial membrane potential ($\Delta\psi$) in muscle mitochondria compared to mitochondria isolated from all tissues (Total). Muscle (#4), Muscle (#8), and Muscle (#10) refer to different extrachromosomal lines expressing blue-fluorescently labeled mitochondria specifically in muscle tissue. *** = $p < 0.0001$ relative to all tissues Total mitochondria control, ‡ = $p < 0.0001$ relative to polarized, mitochondria within an isolate. For polarized mitochondria, $N = 54839$ for Total. 1235 for Muscle(#4), 823 for Muscle(#8), and 618 for Muscle(#10). For depolarized mitochondria $N = 1176$ for Total, 435 for Muscle(#4), 467 for Muscle(#8), and 392 for Muscle(#10).